ROYAL SOCIETY OPEN SCIENCE

rsos.royalsocietypublishing.org

Research

Cite this article: Wang B, Ma B, Song W, Fu Z, Lu Z. 2018 First-principles calculations of structural, electronic, magnetic and elastic properties of Mo_2FeB_2 under high pressure. *R. Soc. open sci.* **5**: 172247.
http://dx.doi.org/10.1098/rsos.172247

Received: 4 January 2018
Accepted: 14 June 2018

Subject Category:
Physics

Subject Areas:
atomic and molecular physics/thermodynamics/nanotechnology

Keywords:
high pressure, electronic properties, magnetism, elastic properties

Authors for correspondence:
Benyuan Ma
e-mail: byma8@126.com
Zhansheng Lu
e-mail: zslu@henannu.edu.cn

First-principles calculations of structural, electronic, magnetic and elastic properties of Mo_2FeB_2 under high pressure

Bin Wang[1], Benyuan Ma[2], Wei Song[1], Zhe Fu[1] and Zhansheng Lu[3]

[1]Physics and Electronic Engineering Department, Xinxiang University, Xinxiang 453003, People's Republic of China
[2]College of Physics and Electronic Engineering, Nanyang Normal University, Nanyang 473061, People's Republic of China
[3]College of Physics and Materials Science, Henan Normal University, Xinxiang 453000, People's Republic of China

BW, 0000-0001-6391-2144

The structural, electronic, magnetic and elastic properties of Mo_2FeB_2 under high pressure have been investigated with first-principles calculations. Furthermore, the thermal dynamic properties of Mo_2FeB_2 were also studied with the quasi-harmonic Debye model. The volume of Mo_2FeB_2 decreases with the increase in pressure. Using the analysis of the density of the states, atom population and Mulliken overlap population, it is observed that as the pressure increases, the B–B bonds are strengthened and the B–Mo covalency decreases. Moreover, for all pressures, Mo_2FeB_2 is detected in the anti-ferromagnetic phase and the magnetic moments decrease with the increase in pressure. The calculated bulk modulus, shear modulus, Young's modulus, Poisson's ratio and universal anisotropy index all increase with the increase in pressure. From thermal expansion coefficient analysis, it is found that Mo_2FeB_2 shows good volume invariance under high pressure and temperature. The examination of the dependence of heat capacity on the temperature and pressure shows that heat capacity is more sensitive to temperature than to pressure.

1. Introduction

Mo_2FeB_2 is widely used as a wear-resistant material owing to its high degree of hardness, high melting point and high electrical

THE ROYAL SOCIETY PUBLISHING

conductivity [1]. Current studies to improve the mechanical properties of Mo_2FeB_2 mainly introduce Mn, Nb, V, Cr, Ni and C [2–7]. Mn addition can improve the wettability of the Fe binder phase on the Mo_2FeB_2 hard phase. This enhancement is observed because Mn can refine the grains, decrease the porosity and increase the phase uniformity of Mo_2FeB_2 [2,6]. Addition of V and Nb can also refine the grains [3,7]. Furthermore, with the increase in the Nb/V content, the hardness and transverse rupture strength are both first enhanced and then decreased [7]. Additions of Cr and Ni enhance the hardness and transverse rupture strength [4]. Addition of carbon can improve the hardness but it decreases the transverse rupture and fracture toughness [5].

Theoretical studies of Mo_2FeB_2 are rare. Using empirical electron theory of solids and molecules, Pang *et al*. predicted that the brittleness of Mo_2FeB_2 arises from weak bonds [8]. He *et al*. found that Mo_2FeB_2 exhibits the largest shear and Young's moduli (E) due to its strong chemical bonding among the Mo_2XB_2 and MoX_2B_4 (X = Fe, Co, Ni) ternary borides with first-principles methods [9]. By the first-principles method, it is also found that addition of Cr can improve the volume deformation resistance of Mo_2FeB_2. Addition of Mn can improve the shear deformation resistance of Mo_2FeB_2 [10]. It is worth pointing out that the structure, electronic density of states (DOS), and magnetic and elastic properties of Mo_2FeB_2 under normal pressure have been studied by us before [11]. It was found that magnetism has a great impact on the crystal structure and mechanical properties. The anti-ferromagnetic (AF) case is the ground state. The B–B and B–Mo bonds play an important role in the shear modulus. The Fe atom contributes the most to the magnetism.

To date, there have been no reports on Mo_2FeB_2 behaviour under high pressure. On the one hand, high temperature and high pressure can help increase the density of the hard phase [12,13]. On the other hand, Mo_2FeB_2-based cermets are typically used in extreme conditions (high pressure and high temperature). The variation of the magnetic properties and structure of Mo_2FeB_2 under high pressure is still unknown. Magnetism will affect the accuracy of the calculation of the crystal structure. Thus, it is necessary to study the electronic structure, elastic properties, magnetic properties and thermodynamic properties of Mo_2FeB_2 under high pressure.

2. Calculation method and crystal structure

The calculation method in this paper was similar to that of previous work [11]. The work was conducted based on density functional theory [14,15] with the calculations performed using the Cambridge Serial Total Energy Package (CASTEP) plane wave code [16]. The interaction of the ionic core and valence electrons was modelled with ultrasoft pseudopotentials. The valence states considered here correspond to B $2s^2 2p^1$, Fe $3d^6 4s^2$ and Mo $4d^5 5s^1$. The generalized gradient approximation in the Perdew–Burke–Ernzerhof form is used to describe the exchange and correlation terms [17,18]. The integration over the Brillouin zone was performed with the Monkhorst and Pack k-point mesh integrations [19]. The cut-off energy was set to 330 eV, and the $5 \times 5 \times 8$ k-point grid was used. The convergence conditions were set as the maximum force on the atom below 0.01 eVÅ^{-1}, the maximum stress below 0.02 GPa and the maximum displacement between the cycles below 0.0005 Å. Hydrostatic pressure was applied in the x, y and z directions simultaneously with an increase of 10 GPa each time. Furthermore, the AF ground state was first set before the geometric optimization. The setting method can be found in [11]. Then, the lattice optimization with spin polarization was performed.

In this work, the unit cell that contains 4 Mo atoms, 2 Fe atoms and 4 B atoms with periodic boundary conditions was used. Mo_2FeB_2 with tetragonal symmetry belongs to the $P4/mbm$ space group. Furthermore, the ground state of Mo_2FeB_2 is AF [11]. The calculated data listed in table 1 agree well with the previous theoretical and experimental results [11,20,21]. The largest error is less than 1.6% between the volume V_0 obtained by our calculations and the experimental data of Gladyshevskii [20].

3. Results and discussion

3.1. Crystal structures under pressure

According to the whole calculation, Mo_2FeB_2 maintained tetragonal symmetry and the $P4/mbm$ space group. Furthermore, the atoms almost keep the same fractional coordinates, and the largest displacement (fractional coordinates) is less than 2% (supporting data). Figure 1 shows the relationship between the

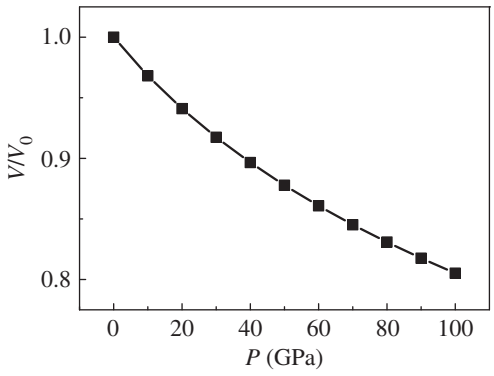

Figure 1. The relationship between normalized volume V/V_0 and pressure for tetragonal Mo_2FeB_2.

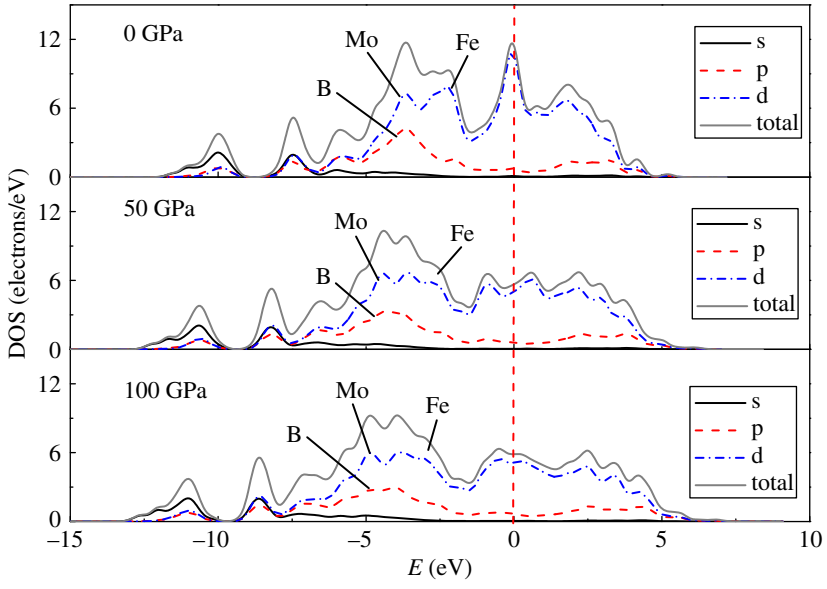

Figure 2. PDOS and TDOS of Mo_2FeB_2 under 0 GPa, 50 GPa and 100 GPa.

Table 1. Calculated equilibrium lattice parameters (*a* and *c*) of Mo_2FeB_2 compared with experimental data and theoretical data.

Mo_2FeB_2	*a*(Å)	*c*(Å)	V_0(Å^3)	*c*/*a*
present	5.748	3.157	104.317	0.549
theoretical [11]	5.743	3.159	104.19	0.550
experimental [20]	5.807	3.142	105.952	0.541
experimental [21]	5.782	3.148	105.242	0.544

normalized volume V/V_0 and the pressure, where V_0 is the equilibrium volume at zero pressure. It can be observed that the volume decreases with increasing pressure.

3.2. Electronic structure and electronic population under pressure

The calculated partial density of states (PDOS) and the total density of states (TDOS) under 0, 50 and 100 GPa around the Fermi level are shown in figure 2. Mo_2FeB_2 retained its metallic character at the Fermi level under different pressures. There are two peaks in the energy range from −15 to −7.5 eV that are composed of 2s and 2p bands of B. This region of the DOS corresponds to the B–B covalent bonds composed of the strongly hybridized B s and p states and gives a positive contribution to the shear

modulus. With the pressure increasing, the two peaks move to lower energy, which means that the B–B bonds are strengthened. The PDOS range from −7.5 eV to −2 eV is predominantly composed of B 2p, Mo 4d and Fe 3d bands. However, this region is mainly composed of the strongly hybridized B p and Mo d states (forming the B–Mo covalent bonds) and the less hybridized B p and Fe d states (forming the B–Fe covalent bonds). As the pressure increases, the energy range of this hybridized region increases, the B p and Fe d hybrids increase and the B–Mo covalency decreases. Around the Fermi level, the DOS are mainly the d bands of Mo and Fe, which form the Fe–Mo, Fe–Fe and Mo–Mo metal ion bonds, making a negative contribution to the shear modulus.

The electronic population can also be used to analyse the electronic structure and the covalent or ionic nature of a bond [22]. A high value of the bond population indicates the strong covalency of a bond. Otherwise, the bond is ionic. The results are listed in table 2, which can be separated into three categories of chemical interactions, namely, B–B, B–Mo(Fe) and Mo(Fe)–Mo(Fe) bonds. All bond lengths decrease as the pressure increases, which is due to the shrinking of the volume. The B–B and B–Fe bond populations increase with increasing pressure, which means that the covalence of the B–B and B–Fe bonds increases. On the other hand, the B–Mo I, B–Mo II, Fe–Mo, Mo–Mo I and Mo–Mo II bond populations decrease with increase in pressure. This finding indicated that the ionicity of the B–Mo I and B–Mo II bonds increases, and the Fe–Mo, Mo–Mo I and Mo–Mo II populations belong to the anti-bonding states. Furthermore, until the pressure reaches 100 GPa, the B–Fe and B–Mo I populations are almost the same. As the pressure increases, B–Mo II changed to anti-bonding. Overall, the B–B bond is the strongest covalent bond, which is in agreement with the results of the DOS analysis (strongly hybridized B s and p states).

3.3. Magnetic properties

As the magnetic properties have significant impact on the crystal structures [11], the magnetic properties of the ground state should be decided. The calculated magnetic properties of Mo_2FeB_2 under different pressures are listed in table 3. In all cases, Mo_2FeB_2 shows AF behaviour. From the data in table 3, it can be found that the magnetic moments decrease with increasing pressure. The strong intra-band exchange interactions of the Fe d orbitals play a critical part in the magnetic moment of Mo_2FeB_2 [11]. There is no magnetic moment for Mo. Figure 3 illustrates the calculated Fe 3d DOS of Mo_2FeB_2 under the pressures of 0, 50 and 100 GPa. The examination of figure 3 also shows that the majority of spin channels are analogous to each other. Two obvious main peaks are present at 0 and −2.5 eV. With the pressure increasing, the heights of the peaks are reduced and the peaks move to lower energy, which is in good agreement with the decrease of the magnetic moment.

3.4. Elastic properties

Elastic constants depend on the stress and the strain tensors according to Hooke's law. The elastic constants C_{ijkl} can be written as follows [23–25]:

$$C_{ijkl} = \left(\frac{\partial \sigma_{ij}(x)}{\partial e_{kl}}\right)_X, \tag{3.1}$$

where e_{kl}, σ_{ij}, X and x are, respectively, the Eulerian strain tensor, the applied stress tensor and the coordinates before and after the deformation. For the tetragonal crystal studied here, six independent elastic constants, C_{11}, C_{33}, C_{44}, C_{66}, C_{12} and C_{13}, can be obtained. The bulk modulus (B) and the shear modulus (G) are deduced from the elastic constants. Based on the Voigt and Reuss method [26], for tetragonal crystals, the bulk modulus and the shear modulus are defined as

$$B_V = \frac{2C_{11} + 2C_{12} + 4C_{13} + C_{33}}{9}, \tag{3.2}$$

$$B_R = \frac{1}{2(S_{11} + S_{12}) + S_{33} + 4S_{13}}, \tag{3.3}$$

$$G_V = \frac{2C_{11} - C_{12} - 2C_{13} + C_{33} + 6C_{44} + 3C_{66}}{15} \tag{3.4}$$

and

$$G_R = \frac{15}{8S_{11} - 4S_{12} - 8S_{13} + 4S_{33} + 6S_{44} + 3S_{66}}. \tag{3.5}$$

The arithmetic average of the Voigt and the Reuss bounds, which is the Voigt–Reuss–Hill (VRH) average, is considered to provide the best estimation of the isotropic elastic moduli [27]. Using the

Table 2. Mulliken overlap population analysis for bonds of Mo_2FeB_2 under different pressures.

	B–B		B–Fe		B–MoI		B–MoII		Fe–Mo		Mo–MoI		Mo–MoII	
P (GPa)	length	population	length	population	length	population	length	population	length	population	length	population	length	population
0	1.83	0.60	2.32	0.16	2.32	0.59	2.33	0.31	2.64	0.04	2.89	0.04	2.99	−1.05
10	1.82	0.61	2.29	0.18	2.30	0.58	2.30	0.27	2.61	−0.01	2.86	0.05	2.96	−1.18
20	1.80	0.61	2.27	0.19	2.27	0.56	2.28	0.23	2.59	−0.06	2.83	0.05	2.93	−1.30
30	1.80	0.62	2.25	0.20	2.26	0.55	2.28	0.21	2.58	−0.09	2.81	0.04	2.91	−1.36
40	1.78	0.62	2.22	0.22	2.23	0.51	2.25	0.16	2.55	−0.18	2.78	0.02	2.88	−1.55
50	1.77	0.63	2.21	0.24	2.22	0.49	2.24	0.12	2.53	−0.25	2.76	0.00	2.85	−1.66
60	1.76	0.63	2.19	0.26	2.20	0.46	2.23	0.09	2.51	−0.32	2.74	−0.03	2.83	−1.78
70	1.75	0.64	2.17	0.27	2.19	0.43	2.21	0.05	2.50	−0.39	2.73	−0.06	2.81	−1.90
80	1.75	0.65	2.16	0.29	2.17	0.40	2.20	0.01	2.48	−0.46	2.71	−0.09	2.79	−2.01
90	1.74	0.66	2.15	0.31	2.16	0.37	2.19	−0.02	2.47	−0.54	2.70	−0.14	2.78	−2.13
100	1.73	0.67	2.13	0.33	2.15	0.34	2.18	−0.06	2.46	−0.62	2.68	−0.19	2.76	−2.25

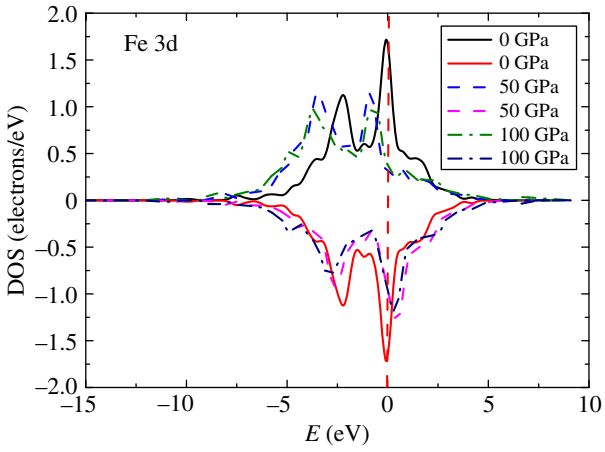

Figure 3. Spin-polarized DOS for Fe d bands of Mo_2FeB_2 under 0 GPa, 50 GPa and 100 GPa. The vertical dashed line at 0 eV is the Fermi level.

Table 3. Magnetic moment of Mo_2FeB_2 at different pressures.

	Fe (hbar/2)	
P (GPa)	up	down
0	2.04	−2.04
10	1.92	−1.92
20	1.81	−1.81
30	1.72	−1.72
40	1.63	−1.63
50	1.55	−1.55
60	1.47	−1.47
70	1.40	−1.40
80	1.33	−1.33
90	1.27	−1.27
100	1.21	−1.21

VRH average, the bulk and the shear modulus can be written as $B = (B_V + B_R)/2$ and $G = (G_V + G_R)/2$, respectively. The average E and Poisson's ratio (υ) can be expressed with B and G as follows [28]:

$$E = \frac{9BG}{3B + G} \tag{3.6}$$

and

$$\upsilon = \frac{E - 2G}{2G}. \tag{3.7}$$

If the elastic constants satisfy the Born stability criterion, the crystal structure is usually considered to be mechanically stable [29,30]. A positive determinant for the crystal's symmetric matrix is required for the criterion of a stable crystal. For tetragonal crystals, the mechanical stability restrictions can be described as

$$\begin{aligned}&(C_{11} - P) > 0, (C_{33} - P) > 0, (C_{44} - P) > 0, (C_{66} - P) > 0,\\ &(C_{11} - C_{12} - 2P) > 0, (C_{11} + C_{33} - 2C_{13} - 4P) > 0,\\ &(2C_{11} + 2C_{12} + C_{33} + 4C_{13} + 3P) > 0.\end{aligned} \tag{3.8}$$

The elastic constants of Mo_2FeB_2 under different pressures are shown in figure 4. It was found that the elastic constants increase almost linearly with increasing pressure up to 100 GPa. This is caused by the enhancement of the covalent bonds (B–B, B–Fe) mentioned above. All elastic constants meet the Born stability criterion, indicating that Mo_2FeB_2 is mechanically stable from 0 to 100 GPa.

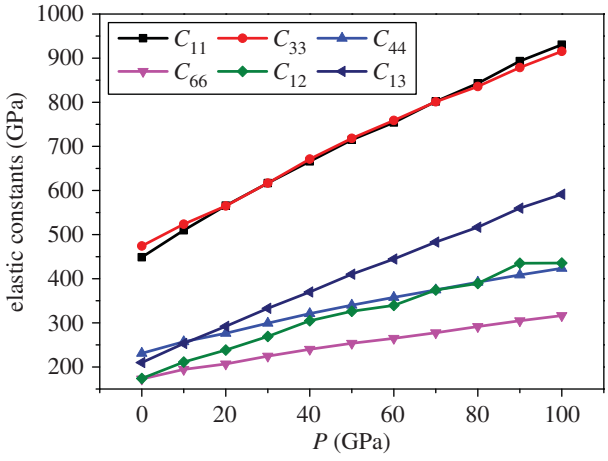

Figure 4. Pressure dependence of elastic constants of Mo_2FeB_2.

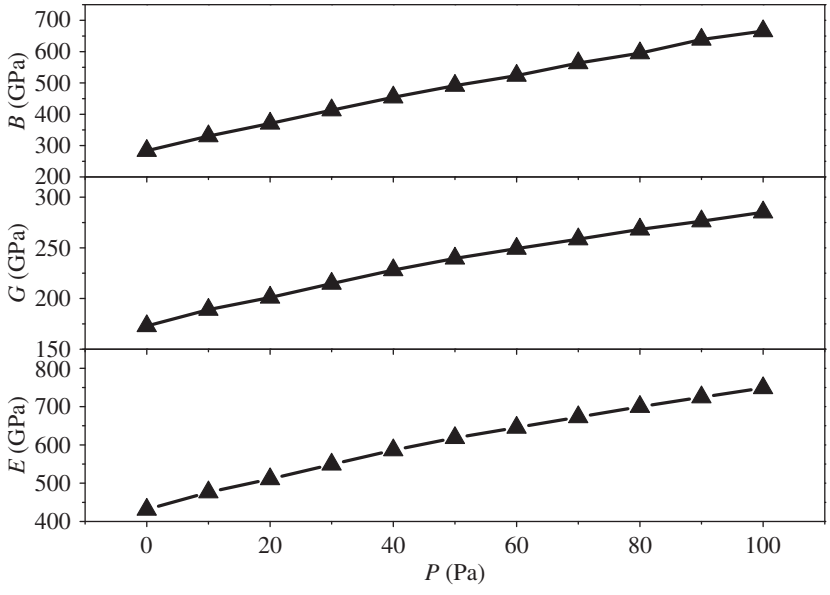

Figure 5. Pressure dependence of the bulk modulus, shear modulus and Young's modulus.

Figure 5 shows a monotonic increase of B with the pressure. This finding means that the resistance ability of the material to uniform compression increases. B can also reflect the average atomic bond strength. Hence, the atomic bond strength of Mo_2FeB_2 increases with the pressure. Furthermore, the values of G and C_{44} of Mo_2FeB_2 also increase monotonically with the increase in pressure, thus indicating that it is harder to achieve a shear deformation with increasing pressure. The higher shear modulus implies the more pronounced directional interatomic bonding [31]. Thus, the bonding behaviour of Mo_2FeB_2 becomes more directional with the increase in pressure. Moreover, E also increases monotonically with the pressure, which means that it is harder to stretch the material uniformly with increasing pressure. As B, G and E increase monotonically with the pressure, the hardness is supposed to have a similar trend. Poisson's ratio, B/G and the universal anisotropy index (A^U) are also calculated here, as shown in figure 6. Poisson's ratio is inversely proportional to the volume change during uniaxial deformation. That is, the lower the υ value, the larger is the volume change. The values of υ increase with the increase in pressure, thus indicating that there is lower volume change during uniaxial deformation. To analyse the ductile (brittle) behaviour of materials, a simple relationship has been proposed by Pugh: a high value of B/G corresponds to malleability, while a low value corresponds to brittleness [32]. It was suggested that 1.75 is the critical value that separates ductile and brittle materials. That is, if $B/G > 1.75$, the material behaves in a ductile manner. As shown in figure 6, Mo_2FeB_2 becomes more ductile as the

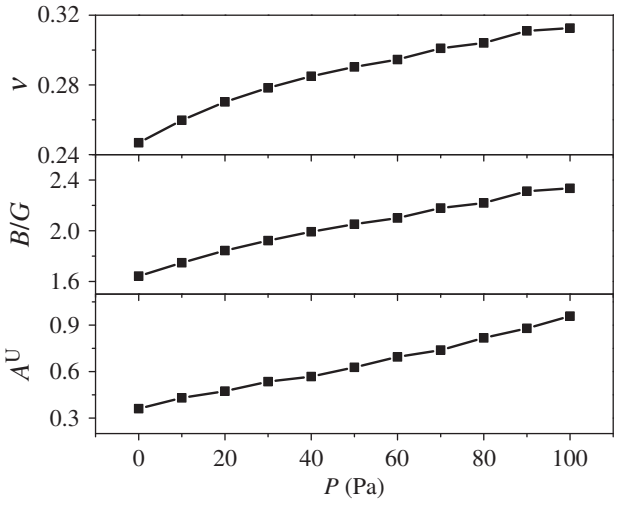

Figure 6. Calculated Poisson's ratio, the ratio of the bulk modulus to the shear modulus and the universal anisotropy index as functions of pressure.

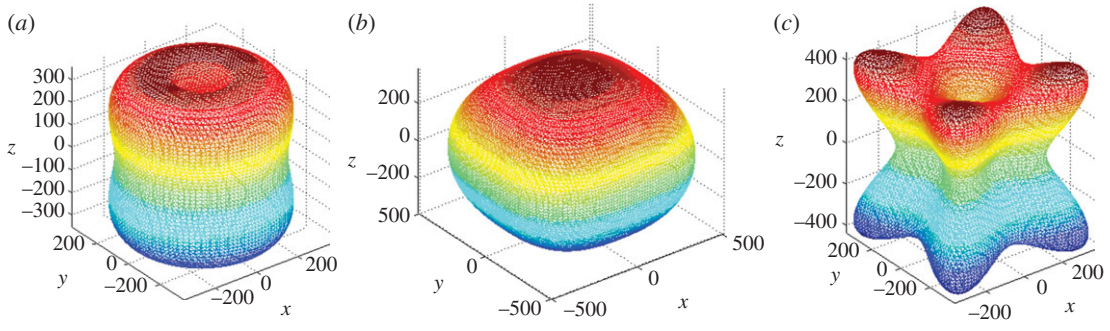

Figure 7. The directional-dependent Young's modulus of Mo_2FeB_2 under different pressures: (*a*) 0, (*b*) 50, (*c*) 100 GPa (the units are all in GPa).

pressure increases. When the pressure increases to 20 GPa, Mo_2FeB_2 changes from brittle to ductile. A^U can be defined as

$$A^U = 5\frac{G_V}{G_R} + \frac{B_V}{B_R} - 6. \tag{3.9}$$

A^U can indicate the degree of anisotropy for crystals. Zero means the crystal is isotropic. It is noted that A^U increases with the pressure, which means that Mo_2FeB_2 is anisotropic under pressure.

In addition, the directional-dependent Young's modulus can also predict the elastic anisotropy of a crystal. For a tetragonal crystal this is expressed as follows [33]:

$$\frac{1}{E} = S_{11}(l_1^4 + l_2^4) + (2S_{13} + S_{44})(l_1^2 l_3^2 + l_2^2 l_3^2) + S_{33} l_3^4 + (2S_{12} + S_{66}) l_1^2 l_2^2, \tag{3.10}$$

where l_1, l_2 and l_3 represent the directional cosines with respect to the *x*-, *y*- and *z*-axes, respectively. Using the compliance constant S_{ij}, the directional Young's moduli for Mo_2FeB_2 were obtained, as shown in figure 7. For direct comparison, the directional-dependent Young's moduli are plotted in figure 7 for the pressures of 0, 50 and 100 GPa.

A spherical curved surface represents an isotropic system, while the deviation from the spherical shape indicates the extent of elastic anisotropy. For Mo_2FeB_2 at 0 GPa, the curved surface deviates slightly from the spherical shape, which means that there is a slight elastic anisotropy for Mo_2FeB_2, which is in agreement with the discussion above. When the pressure increased to 50 GPa, the curved surface changed to oval. This indicates that the elastic anisotropy increased. Furthermore, when the pressure reaches 100 GPa, the curved surface has a larger distortion, thus indicating larger anisotropy.

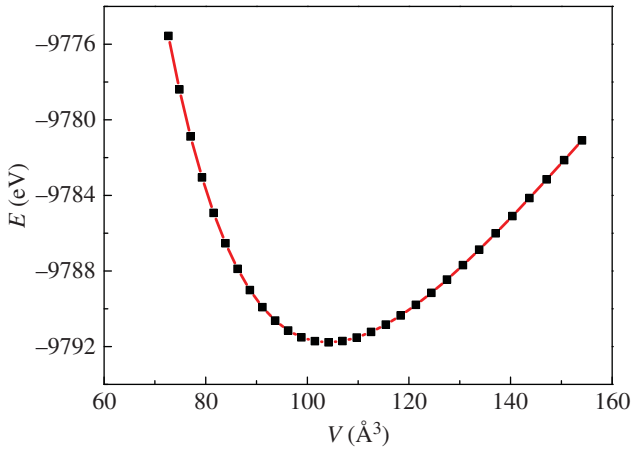

Figure 8. The correlation of the total energy (E) and unit cell (V) of Mo_2FeB_2. The black squares are the calculated values and the red line is the fitted curve with the Birch–Murnaghan EOS.

3.5. Thermal properties

To study the thermodynamic properties of Mo_2FeB_2 under high pressures, a quasi-harmonic Debye model [34] was used, in which the non-equilibrium Gibbs function $G^*(V; p, T)$ can be expressed as follows [35]:

$$G^*(V;p,T) = E(V) + pV + A_{\text{vib}}[\Theta(V);T], \tag{3.11}$$

where $E(V)$ is the total energy per unit cell, pV is the constant hydrostatic pressure condition, $\Theta(V)$ is the Debye temperature and A_{vib} is the vibrational term. A_{vib} can be expressed with the Debye model of the phonon DOS as follows [36]:

$$A_{\text{vib}}(\Theta;T) = nk_{\text{B}}T\left[\frac{9}{8}\frac{\Theta}{T} + 3\ln(1-\mathrm{e}^{-\Theta/T}) - D\left(\frac{\Theta}{T}\right)\right]. \tag{3.12}$$

Here, n is the number of atoms per formula unit, and $D(\Theta/T)$ represents the Debye integral. For an isotropic solid, Θ is defined as follows [34]:

$$\Theta = \frac{\hbar}{k_{\text{B}}}[6\pi^2 V^{1/2} n]^{1/3} f(\sigma)\sqrt{\frac{B_{\text{s}}}{M}}, \tag{3.13}$$

where M is the molecular mass per unit cell and B_{s} is the adiabatic bulk modulus, which is approximately given by the static compressibility [34]

$$B_{\text{s}} \approx B(V) = V\left(\frac{\mathrm{d}^2E(V)}{\mathrm{d}V^2}\right). \tag{3.14}$$

$f(\sigma)$ is written as [37]

$$f(\sigma) = \left\{3\left[2\left(\frac{21+\sigma}{31-\sigma}\right)^{3/2} + \left(\frac{11+\sigma}{31-\sigma}\right)^{3/2}\right]^{-1}\right\}^{1/3}, \tag{3.15}$$

where σ is the Poisson's ratio. Thus, the thermal equation of state (EOS) $V(P,T)$ can be calculated by the following equation with respect to volume V:

$$\left(\frac{\partial G^*(V;p,T)}{\partial V}\right)_{p,T} = 0. \tag{3.16}$$

The heat capacity C_V and the thermal expansion coefficient α are defined as

$$C_{V,\text{vib}} = 3nk_{\text{B}}\left[4D\left(\frac{\Theta}{T}\right) - \frac{3\Theta/T}{\mathrm{e}^{\Theta/T}-1}\right] \tag{3.17}$$

$$\alpha = \frac{\gamma C_v}{B_{\text{T}}V}, \tag{3.18}$$

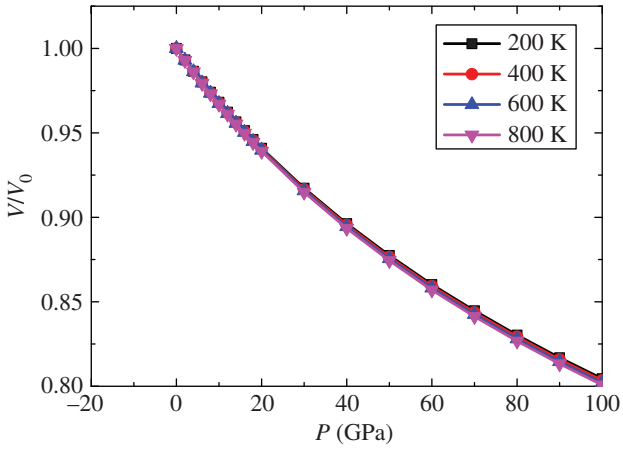

Figure 9. The normalized volume V/V_0 as a function of pressure at temperature 200, 400, 600 and 800 K.

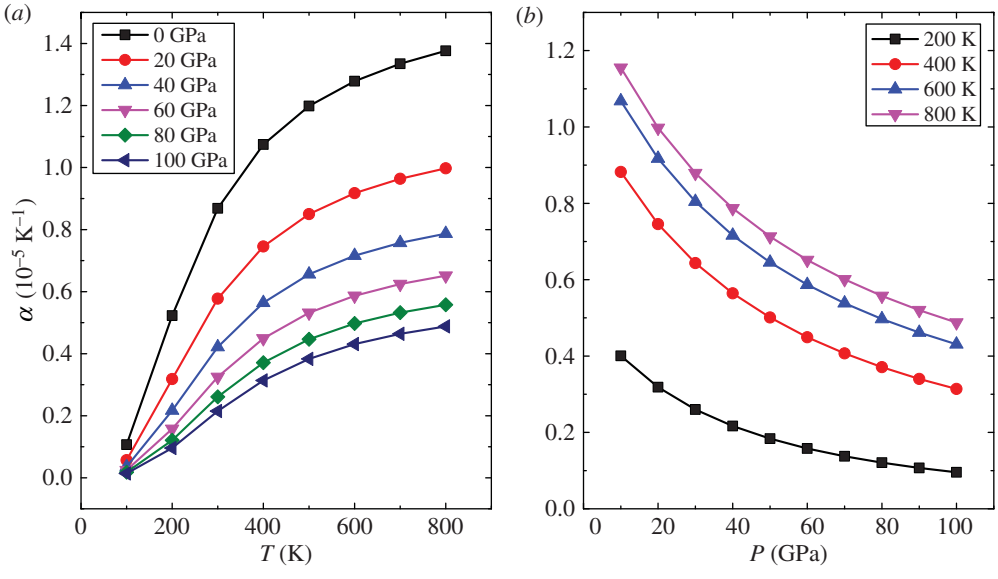

Figure 10. The thermal expansion as a function of temperature (*a*) and pressure (*b*).

where B_T is the isothermal bulk modulus and γ is the Grüneisen parameter, which is expressed as

$$\gamma = -\frac{\mathrm{d}\ln\Theta(V)}{\mathrm{d}\ln V}. \tag{3.19}$$

This paper calculated the pressure dependence of thermodynamic properties in the 0–100 GPa pressure range. First, a series of lattice constants were selected. Then, the corresponding unit cell volume and total energy were calculated and the third-order Birch–Murnaghan state equation was used for curve fitting to obtain the *E*–*V* curve (figure 8). As seen in the figure, the calculated values agreed well with the fitted values.

The dependence of the calculated normalized volume V/V_0 on pressure P and temperature T is illustrated in figure 9, where V_0 is the zero-pressure equilibrium volume. It is found that V/V_0 decreases due to the increase in pressure and the slope of the curves also decreases, thus indicating that Mo_2FeB_2 is increasingly difficult to compress as the pressure increases. It is also found that the curves changed little with the increase in pressure, which means that Mo_2FeB_2 is stable under different temperatures.

The thermal expansion coefficient (α) can intuitively reflect a material's structural stability. Figure 10 shows the dependence of α on pressure and temperature. For a given pressure (figure 10*a*), α increases rapidly especially at zero pressure below a temperature of 400 K, and it increases slowly at higher temperatures. This is an expression of the excellent volume invariance under high temperature.

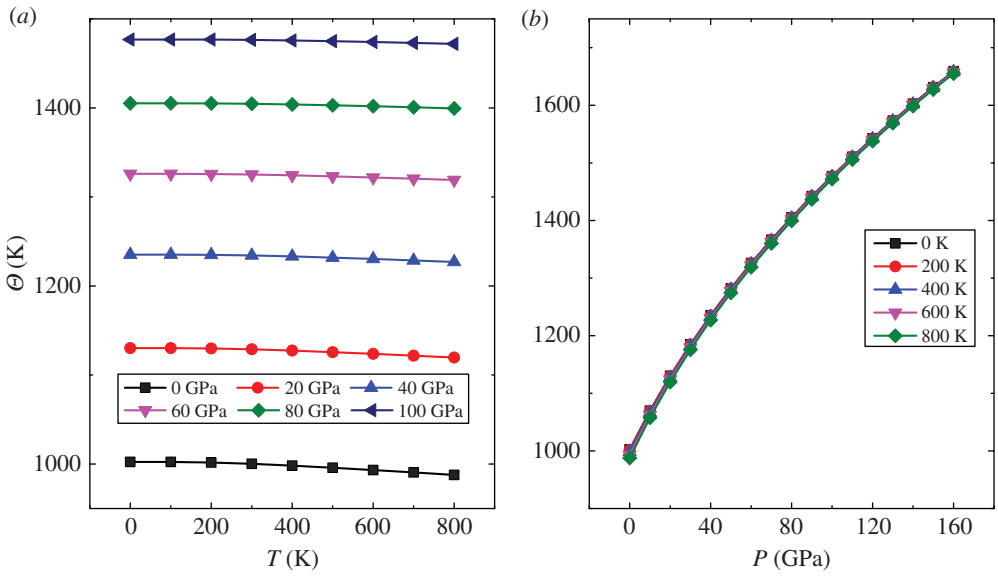

Figure 11. The Debye temperature as a function of temperature (*a*) and pressure (*b*).

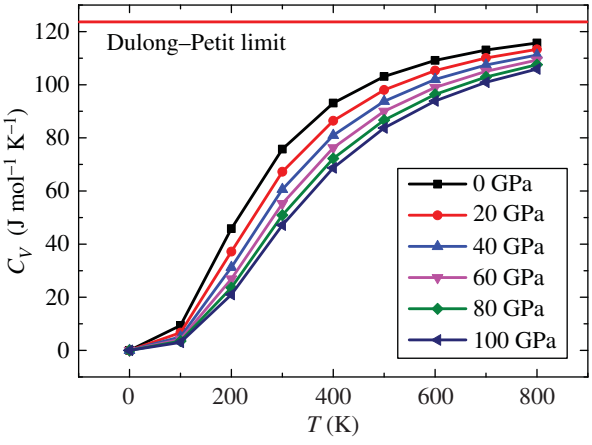

Figure 12. Temperature dependence of the heat capacity at different pressures.

However, α decreases strongly below 40 GPa with pressure at a constant temperature (figure 10*b*). Moreover, it decreases slowly above 40 GPa with the increase in pressure. This indicates that Mo_2FeB_2 possesses good volume invariance under high pressure.

Figure 11 shows the Debye temperature (Θ) as a function of the temperature and pressure. At room temperature ($T = 300$ K), Θ of 1000.19 K is obtained. Unfortunately, we did not find the corresponding experimental data. Under the application of pressure, Θ decreases very slowly with increase in temperature (figure 11*a*). Furthermore, at a given temperature (figure 11*b*), Θ tends to increase linearly with the increase in pressure. This indicated that the influence of the pressure on Θ is strong and that Θ is less affected by the temperature. The Debye temperature can also reflect the bonding between atoms. Thus, with the increase in pressure, the strength of atoms' bonds increases, which is consistent with the above analysis.

Heat capacity C_V is one of the most important parameters in thermodynamics. Figure 12 shows the relationship between the heat capacity and temperature under different pressures. For the same pressure, C_V increases with the temperature. For the same temperature, C_V decreases with the increase in pressure, thus implying that increasing the pressure is equivalent to reducing the temperature. The relationships of C_V with the temperature and pressure show that C_V is more sensitive to temperature than to the pressure. Owing to the anharmonic effect, when $T < 500$ K, the variation of C_V with the changes in the

temperature and pressure is more obvious. Under high temperature and high pressure, the heat capacity approaches the Dulong–Petit limit.

4. Conclusion

First-principles calculations were performed to investigate the structure, electronic DOS, and magnetic and elastic properties of Mo_2FeB_2 under high pressure. The volume of Mo_2FeB_2 decreases almost linearly with the increase in pressure. Examination of the DOS showed that with the pressure increasing, the B–B bonds were strengthened and the B–Mo covalency decreased. The atom population analysis and Mulliken overlap population analysis also found these results. With the pressure increasing, the sp hybridization of the B atoms increases, resulting in the increase of strong covalent bonding between the B atoms (forming a B–B bond). Moreover, the B–B and B–Fe bond populations increase with the increase in pressure, thus implying that the covalence of the B–B and B–Fe bonds increases. The analysis of the magnetic properties shows that, for all pressures, Mo_2FeB_2 shows AF behaviour and the magnetic moments decrease with the increase in pressure. The calculated B, G, E, B/G, v and A^U all increase with the increase in pressure, which means that the hardness and ductility of Mo_2FeB_2 increase with the increase in pressure. Furthermore, from the directional-dependent Young's modulus of Mo_2FeB_2 under different pressures, it is found that elastic anisotropy increases with the increase in pressure. A quasi-harmonic Debye model was used to investigate the thermodynamic properties of Mo_2FeB_2 under high pressures. As the pressure increases, Mo_2FeB_2 is increasingly hard to compress. Furthermore, Mo_2FeB_2 is stable under different temperatures. From α analysis, it is found that Mo_2FeB_2 possesses good volume invariance under high pressure and temperature. The value of Θ is more influenced by pressure than by temperature. The examination of the relationships of C_V with the temperature and pressure shows that C_V is more sensitive to temperature than to pressure.

Data accessibility. The data have been deposited at the Dryad Digital Repository (http://dx.doi.org/10.5061/dryad.8t70r) [38].

Authors' contributions. B.M and Z.L conceived and designed this work. B.W. carried out this work, acquired the data and prepared the draft. All the authors equally analysed the results and approved the final version of the manuscript.

Competing interests. We declare we have no competing interests.

Funding. The authors are grateful for the support provided by the Science Fund of Educational Department of Henan Province of China (grant nos. 15A140032, 15A140030 15B150010 and 18B430012), the Key Scientific and Technological Project of Technology Department of Henan Province of China (grant no. 162102210305), Project of Technology Department of Henan Province of China (grant no. 152102210201), Xinxiang University Science and Technology Innovation Fund (grant no. 15ZP01 and 15ZB25), Xinxiang University Doctor Initial Research Program (grant no. 1366020018 and 1366020039) and the Ninth Group of Key Disciplines in Henan Province (grant no. 2018119).

References

1. Takagi K-i. 2006 Development and application of high strength ternary boride base cermets. *J. Solid State Chem.* **179**, 2809–2818. (doi:10.1016/j.jssc.2006.01.023)
2. Yu H, Zheng Y, Liu W, Zheng J, Xiong W. 2010 Effect of Mn content on the microstructure and mechanical properties of Mo_2FeB_2 based cermets. *Int. J. Refract. Met. Hard Mater.* **28**, 286–290. (doi:10.1016/j.ijrmhm.2009.11.001)
3. Yu H, Zheng Y, Liu W, Zheng J, Xiong W. 2010 effect of V content on the microstructure and mechanical properities of Mo_2FeB_2 based cermets. *Mater. Des.* **31**, 2680–2683. (doi:10.1016/j.matdes.2009.11.051)
4. Wang Q, Pan Y, Hu B, Zhou L. 2011 Effects of alloys on microstructure and properties of Mo_2FeB_2 based cermets. *Adv. Mater.Res.* **399–401**, 399–402.
5. Yu H, Liu W, Zheng Y. 2011 Effect of carbon content on the microstructure and mechanical properties of Mo_2FeB_2 based cermets. *Int. J. Refract. Met. Hard Mater.* **29**, 724–728. (doi:10.1016/j.ijrmhm.2011.06.001)
6. Yang F, Wu Y, Han J, Meng J. 2016 Microstructure, mechanical and tribological properties of Mo_2FeB_2 based cermets with Mn addition. *J. Alloys Compd.* **665**, 373–380. (doi:10.1016/j.jallcom.2016.01.053)
7. Ke D, Pan Y, Xu Y, Yang L, Wu R, Lu Z. 2016 Microstructure and mechanical properties of Mo_2FeB_2 ceramic-steels with Nb/V addition. *Adv.Appl. Ceram.* **116**, 92–98. (doi:10.1080/17436753.2016.1251049)
8. Pang X, Zheng Y, Wang S, Wang Q. 2009 Effect of Mn on valence-electron structure and properties of hard phase in Mo_2FeB_2-based cermets. *Int. J. Refract. Met. Hard Mater.* **27**, 777–780. (doi:10.1016/j.ijrmhm.2009.01.004)
9. He T, Jiang Y, Zhou R, Feng J. 2015 The electronic structure, mechanical and thermodynamic properties of Mo_2XB_2 and MoX_2B_4 (X = Fe, Co, Ni) ternary borides. *J. Appl. Phys.* **118**, 075902. (doi:10.1063/1.4928628)
10. Lin Y, Tong C, Pan Y, Liu W, Singh A. 2017 Elastic properties and electronic structure of Mo_2FeB_2 alloyed with Cr, Ni and Mn by first-principles calculations. *Mod. Phys. Lett. B* **31**, 1750138. (doi:10.1142/S021798491750138X)
11. Wang B, Liu Y, Ye J, Wang J. 2013 Electronic, magnetic and elastic properties of Mo_2FeB_2: first-principles calculations. *Comput. Mater. Sci.* **70**, 133–139. (doi:10.1016/j.commatsci.2012.12.023)
12. Holt J, Munir Z. 1986 Combustion synthesis of titanium carbide: theory and experiment. *J. Mater. Sci.* **21**, 251–259. (doi:10.1007/BF01144729)
13. Zhang L, Huang Z, Shen Y, Guo L. 2017 Bulk Mo_2FeB_2 based cermets fabricated by mechanical ball milling and reaction boronizing sintering. *Powder Metall. Met. Ceram.* **55**, 665–675. (doi:10.1007/s11106-017-9854-z)
14. Hohenberg P, Kohn W. 1964 Inhomogeneous electron gas. *Phys. Rev.* **136**, B864–B871. (doi:10.1103/PhysRev.136.B864)
15. Kohn W, Sham L. 1965 Self-consistent equations including exchange and correlation effects. *Phys. Rev.* **140**, A1133–A1138. (doi:10.1103/PhysRev.140.A1133)
16. Clark S, Segall M, Pickard C, Hasnip P, Probert M, Refson K, Payne M. 2005 First principles methods using CASTEP. *Z. Kristallogr.– Cryst. Mater.* **220**, 567–570. (doi:10.1524/zkri.220.5.567.65075)

17. Perdew J, Burke K, Ernzerhof M. 1996 Generalized gradient approximation made simple. *Phys. Rev. Lett.* **77**, 3865–3868. (doi:10.1103/PhysRevLett.77.3865)
18. Perdew J, Burke K, Ernzerhof M. 1998 Perdew, Burke, and Ernzerhof reply. *Phys. Rev. Lett.* **80**, 891. (doi:10.1103/PhysRevLett.80.891)
19. Monkhorst H, Pack J. 1976 Special points for Brillouin-zone integrations. *Phys. Rev. B* **13**, 5188–5192. (doi:10.1103/PhysRevB.13.5188)
20. Gladyshevskii EI, Fedorov TF, Kuz'ma YB, Skolozdra RV. 1966 Isothermal section of the molybdenum-iron-boron system. *Sov. Powder Metall. Met. Ceram.* **5**, 305–309.
21. Rieger W, Nowotny H, Senesovsky F. 1964 Die Kristallstruktur von Mo_2FeB_2. *Monatsh. Chem.* **95**, 1502–1503.
22. Aouadi S. 2006 Structural and mechanical properties of TaZrN films: experimental and ab initio studies. *J. Appl. Phys.* **99**, 053507. (doi:10.1063/1.2178394)
23. Wang J, Li J, Yip S, Phillpot S, Wolf D. 1995 Mechanical instabilities of homogeneous crystals. *Phys. Rev. B* **52**, 12 627–12 635. (doi:10.1103/PhysRevB.52.12627)
24. Wallace D. 1998 *Thermodynamics of crystals*. New York, NY: Courier Corporation.
25. Karki B, Ackland G, Crain J. 1997 Elastic instabilities in crystals from ab initio stress–strain relations. *J. Phys. Condens. Matter* **9**, 8579. (doi:10.1088/0953-8984/9/41/005)
26. Reuss A. 1929 Calculation of the flow limits of mixed crystals on the basis of the plasticity of monocrystals. *Z. Angew. Math. Mech.* **9**, 49–58. (doi:10.1002/zamm.19290090104)
27. Hill R. 1952 The elastic behaviour of a crystalline aggregate. *Proc. Phys. Soc. A* **65**, 349–354. (doi:10.1088/0370-1298/65/5/307)
28. Kart S, Cagın T. 2010 Elastic properties of Ni_2MnGa from first-principles calculations. *J. Alloys Compd.* **508**, 177–183. (doi:10.1016/j.jallcom.2010.08.039)
29. Sin'Ko G, Smirnov N. 2002 Ab initio calculations of elastic constants and thermodynamic properties of bcc, fcc, and hcp Al crystals under pressure. *J. Phys. Condens. Matter* **14**, 6989–7006. (doi:10.1088/0953-8984/14/29/301)
30. Sin'ko G, Smirnov N. 2004 On elasticity under pressure. *J. Phys. Condens. Matter* **16**, 8101–8104. (doi:10.1088/0953-8984/16/45/032)
31. Zhang X, Jiang Z, Hou Y, Li L. 2009 Elastic properties of $NaXH_4$ (X = B, Al). *J. Phys. Condens. Matter* **21**, 275401. (doi:10.1088/0953-8984/21/27/275401)
32. Pugh S. 2009 XCII. Relations between the elastic moduli and the plastic properties of polycrystalline pure metals. *Lond. Edinb. Dublin Philos. Mag. J. Sci.* **45**, 823–843. (doi:10.1080/14786440808520496)
33. Nye J. 1985 *Physical properties of crystals*. Oxford, UK: Oxford University Press.
34. Blanco M, Francisco E, Luaña V. 2004 GIBBS: isothermal-isobaric thermodynamics of solids from energy curves using a quasi-harmonic Debye model. *Comput. Phys. Commun.* **158**, 57–72. (doi:10.1016/j.comphy.2003.12.001)
35. Otero-de-la-Roza A, Abbasi-Pérez D, Luaña V. 2011 Gibbs2: a new version of the quasiharmonic model code. II. Models for solid-state thermodynamics, features and implementation. *Comput. Phys. Commun.* **182**, 2232–2248. (doi:10.1016/j.cpc.2011.05.009)
36. Blanco M, Pendás A, Francisco E, Recio J, Franco R. 1996 Thermodynamical properties of solids from microscopic theory: applications to MgF_2 and Al_2O_3. *J. Mol. Struc. Theochem* **368**, 245–255. (doi:10.1016/S0166-1280(96)90571-0)
37. Francisco E, Blanco M, Sanjurjo G. 2001 Atomistic simulation of SrF_2 polymorphs. *Phys. Rev. B* **63**, 094107. (doi:10.1103/PhysRevB.63.094107)
38. Wang B, Ma B, Song W, Fu Z, Lu Z. 2018 Data from: First-principles calculations of structural, electronic, magnetic and elastic properties of Mo_2FeB_2 under high pressure. Dryad Digital Repository. (http://dx.doi.org/10.5061/dryad.8t70r)